

# The first kinematic determination of million-year precession period of AGNs

B.P. Gong<sup>1</sup>, Y.P. Li<sup>1</sup>, H.C. Zhang<sup>2</sup>

Received 2011 May 12; accepted \_\_\_\_\_

---

<sup>1</sup>Department of Physics, Huazhong University of Science and Technology, Wuhan 430074, China

<sup>2</sup>Department of Physics and Astronomy, The Ohio University, Athens, OH 45701, USA

## ABSTRACT

Short precession periods like 164d of SS433 can be well determined by observations of time scales longer or much longer than the precession period. However, it doesn't work for sources with precession periods of millions of years. This paper utilizes the particular morphologies of X-shaped sources, so that the 3 dimension kinematics of lobes can be obtained. Thus, for the first time, the million-year precession period of X-shaped sources by observer on the Earth can be determined elegantly:  $(6.1 \pm 1.5)\text{Myr}$ ,  $(1.8 \pm 0.5)\text{Myr}$ , and  $(3.2 \pm 1.2)\text{Myr}$  for 3C52, 3C223.1 and 4C12.03 respectively. The result naturally explains the asymmetry displayed in the morphology of these sources, and the effect of propagation time on the diversity of morphologies is well demonstrated. The precession period may originate from long-term effects of a binary super-massive black hole system, which is a potential source of gravitational wave radiation.

*Subject headings:* galaxies: active — galaxies: jets

## 1. Introduction

First discovered in 1974 (Hogbom & Carlsson 1974) and growing rapidly in recent years (Cheung 2007), the peculiar radio morphologies, X-shaped extragalactic radio sources, are characterized by two low surface brightness wings oriented at an angle to the high surface brightness lobes, giving the total an X-shape. Recently, X-shaped galaxies are being considered as potential transition between Fanaroff-Riley (FR) type I and II (Landt et al. 2010).

Several formation scenarios have been proposed. One is the back-flow of plasma from the active lobes into the wings (Leahy & Williams 1984; Capetti et al. 2002; Hodges-Kluck & Reynold 2011), with subsequent buoyant expansion. It has been argued that the expansion of wings is subsonic, and it becomes untenable for X-shaped sources with wings longer than the active lobes (Dennett-Thorpe et al. 2002). The second scenario is the conical precession of the jet axis (Parma et al. 1985; Mack et al. 1994), which implies a scenario of ballistic jet motion plus jet precession, predicting spiral pattern. However, this model requires a specific accident of the positions at which the source first switched on and its position now. Moreover, it can not explain the notable asymmetry in 3C223.1 (Dennett-Thorpe et al. 2002).

Other two explanations have received much attention lately. They are in agreement that the wings are the relics left over from a rapid realignment of a central super-massive black-hole (SMBH) accretion disk system. The realignment can be a result of a relatively recent merger of a super-massive binary black hole (SMBBH) (Merritt & Ekers 2002; Mezcua et al. 2011) or due to disk-instability (Dennett-Thorpe et al. 2002).

Nevertheless, in these two scenarios the morphology of X-sources apparently requires a rapid change of jet orientation. A number of X-sources have companion galaxies (Dennett-Thorpe et al. 2002), and the host galaxy of 3C293 shows clearly

interaction. Moreover, the double-peaked low-ionization emission lines in the nucleus of a galaxy associated with X-shaped structure (Zhang et al. 2007) provide an interesting signature of link between X-source and SMBBH. Such a link makes X-sources potential sources of gravitational wave radiation, which leads to a steep surge of interest in them recently (Komossa 2003), although they have been known for decades.

In fact, both the jet precession and reorientation scenarios agree that the wings are relics of the previous jet, and the lobes are produced by jet in action. Thus, regardless of the mechanism of the change of the jet axis, We establish a coordinate system, in which the 2-dimensional morphology can be fitted by the simplest geometry. And together with the constraint imposed by the simultaneous arrival time of photons from the south and north lobes of an X-source, the most collimated components of Fig. 1, the 3-dimensional kinematics of the morphology can be obtained. Consequently, the time scale of the formation of the X-shaped morphology (wing and lobe) can be determined in a general manner. Applying to three X-sources of FR-II, 3C52, 3C223.1 and 4C12.03 (Merritt & Ekers 2002; Dennett-Thorpe et al. 2002; Lal & Rao 2007) as shown in Fig. 1, the precession periods (by Earth observer) of  $(6.1 \pm 1.5)\text{Myr}$ ,  $(1.8 \pm 0.5)\text{Myr}$ , and  $(3.2 \pm 1.2)\text{Myr}$  are obtained respectively. Throughout this letter we assume a  $\Omega_\Lambda=0.73$ ,  $\Omega_m=0.27$  cosmology with  $H_0=71\text{km s}^{-1}\text{Mpc}^{-1}$ . And the red-shift,  $z$ , of 3C52, 3C223.1 and 4C12.03 are 0.2854, 0.1074 and 0.1570 respectively (Merritt & Ekers 2002; Saripalli & Subrahmanyan 2009).

## 2. The New Approach

The non-ballistic model (Gong 2008) has been used to interpret the non-radial jet motions of AGNs (Kellermann et al. 2004; Agudo et al. 2007; Lister et al. 2009), in which a knot can be produced by a continuous jet interacting with ambient matter in different directions during the precession of the jet axis. Approximately equal knot-core

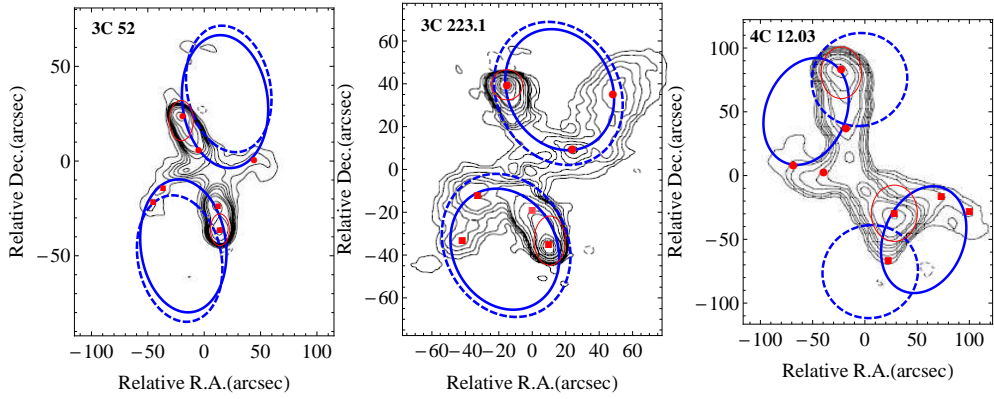


Fig. 1.— The observed morphology of three X-shaped sources(Lal & Rao 2007), and the fitted traces (ellipses) given by the non-ballistic model.The north is to up, and the east is to left. The solid ellipses correspond to the best fit parameters of Table 1, and the dashed ellipses correspond to 20% increase in parameters,  $I$ ,  $\lambda$ , and  $\xi$  (while holding others constant) for 3C52, 3C223.1 and 4C12.03 respectively. The red dots represent components of a morphology which the ellipses try to fit. The red circles are “radius” of the lobes through which the error in precession phase is estimated.

separation is expected when the power of the jet and matter density of the surrounding medium are unchanged in different directions. Such a constant core-knot separation avoids the specific accident of the positions required by conical precession model. And due to the X-shaped morphologies display similar non-radial characteristic as other AGN sources, it is conceivable to apply the non-ballistic model to the X-sources.

This model can be described by two simple geometric equations. Projecting a knot,  $i$ , with knot-core separation,  $R^i$ , to the coordinate system  $x - y - z$ , we have,

$$\begin{aligned}
 R_x^i &= R^i [\sin \lambda \sin I \cos \eta^i + \cos \lambda \cos I], \\
 R_y^i &= R^i [\sin \lambda \sin \eta^i], \\
 R_z^i &= R^i [\cos \lambda \sin I - \sin \lambda \cos I \cos \eta^i],
 \end{aligned} \tag{1}$$

where  $\lambda$ ,  $I$ ,  $\eta$ , and  $R$ , represent the opening angle of the precession cone, the inclination angle between the jet rotation axis and the line of sight (LOS), the precession phase, and the knot-core distance respectively, as shown in Fig. 2.

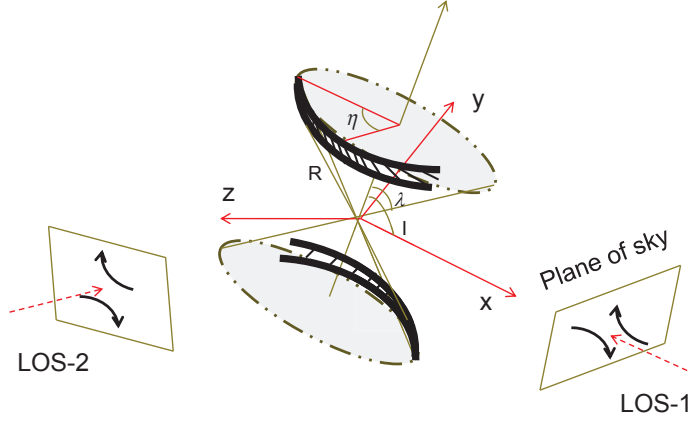


Fig. 2.— Schematic illustration showing an X-shaped source under the non-ballistic precession scenario. Different precession states of the X-sources are equivalent to the observation of one source at different view angles as  $\text{LOS}_1$  and  $\text{LOS}_2$ , and hence different morphologies.

In Eq. (1) the  $x$ -axis is towards the observer. Rotating around the  $x$ -axis for angle  $\xi$ , so that the new  $y$ -axis ( $\Delta\delta$ ) will point north, and the new  $z$ -axis ( $\Delta\alpha$ ) will point east. Therefore, the coordinate of a feature in the plane of sky is given,

$$\begin{aligned} R_\alpha^i &= R^i[\sin \lambda \sin \eta^i] \sin \xi + R^i[\cos \lambda \sin I - \sin \lambda \cos I \cos \eta^i] \cos \xi, \\ R_\delta^i &= R^i[\sin \lambda \sin \eta^i] \cos \xi - R^i[\cos \lambda \sin I - \sin \lambda \cos I \cos \eta^i] \sin \xi, \end{aligned} \quad (2)$$

Eq. (1) predicts an ellipse, the shape of which is determined by four parameters,  $\xi$ ,  $\lambda$ ,  $I$ , and  $R$ . Searching in the parameter space of them as shown in the brackets of Table 1, the best combination of parameters corresponding to the solid ellipses in Fig. 1 can be found.

Once the best fit ellipse for a morphology is found, the precession phase of a knot,

$\eta^i = \Omega t + \eta_0^i$ , can be given, where  $\Omega$  is the precession velocity of a jet, and  $\eta_0^i$  is the initial phase of a knot. However, the precession time,  $t$ , and the precession velocity,  $\Omega$ , can not be separated from  $\eta^i$ . In other words,  $\Omega$  can not be obtained by such a 2-dimensional morphology fitting alone.

Fortunately, a simple constraint can be found to split  $\Omega$  and  $t$ , and therefore allows us to determine the precession period by 3-dimension kinematic. The time of emission of a photon from a knot,  $t_{emit}^i$ , can be measured in the reference frame at rest to the core of an X-shaped source. This photon can reach an observer on Earth at,  $t_{arr} = t_{emit}^i + d/c - x^i/c$ , where  $d$  is the core-observer distance, and  $x^i$ , which is equivalent to  $R_x^i$  of Eq. (1) is the projection of the knot-core separation onto LOS. For simplicity, we can define a time,  $t_a = t_{arr} - d/c$ , so that the time taken for a photon from a knot to the observer can be represented simply by,  $t_a = t_{emit}^i - x^i/c$ .

Also measured in the reference frame at rest to the core of an X-shaped source, the precession time of a knot can be synchronized to the emitting time,  $t^i = t_{emit}^i$ , where  $t^i$  is given by  $\eta^i = \Omega t^i + \eta_0^i$ . Thus, the condition of observing the two signals from two opposite lobes ( $i = 1, 2$  denote the north and south lobe respectively) at the same time becomes:

$$t^i - x^i/c = t_a. \quad (3)$$

Certain precession phases result in,  $t^i - x^i/c > t_a$ , which means that the signal has not arrived to the observer yet, and is hence unobservable, whereas,  $t^i - x^i/c < t_a$  means that the received signal is from a knot that has been at its emitting site for a period of time. If it has afterglow emission that is above the threshold of detection, then it is still observable.

Therefore, a knot which is unobservable in the case of zero cooling time,  $t^i - x^i/c < t_a$ , becomes detectable provided the emissivity of the knot is above the threshold of detection in the cooling time,  $t_c^i$ . Such an emission reaches the Earth at:

$$t_c^i + t^i - x^i/c = t_a. \quad (4)$$



Consequently, with larger and larger separation of the active lobes, a knot in the wings corresponds to larger and larger  $t_c^i$ , so that it appears more diffused and faint until it becomes unobservable.

Limited by the expansion speeds of low-luminosity FR-II sources, the advance speeds of X-sources are likely not greater than  $0.04c$  (Dennett-Thorpe et al. 2002). Such non-relativistic speeds correspond to a negligible Doppler boosting effect, so that the flux of a knot depends primarily on the emissivity. Hence, the precession period at the frame of the source,  $P_p$ , and at the Earth,  $P_p^{obs}$ , are related by  $P_p(1+z) = P_p^{obs}$ , where  $z$  is the red-shift of the source.

Multiplying the precession velocity,  $\Omega$ , at the two sides of Eq. (3), we have,

$$\eta^i - \eta_0^i - \Omega x^i / c = \eta_a, \quad (5)$$

where  $\eta_a = \Omega t_a$ . Apparently, an X-source is observed when the photons from the lobes arrive at the Earth simultaneously. At this moment the initial phases of the two lobes can be treated as,  $\eta_0^1 = \eta_0^2$ , without losing generality. Thus  $\eta_0^i$  of Eq. (5) can be canceled.

The  $\eta^i$  and  $x^i$  of the north and south components can be obtained by fitting the 2-dimensional X-shaped morphology. The process is simply putting the geometrical parameters of Table 1 (except  $\Omega$  and  $\Omega^{obs}$ ) into Eq. (2), then find the best-fit parameters through minimizing the sum of the square of the residuals of the predicted ellipse from the observed morphologies. The pair ellipses (with same group of geometric parameters) for each source are required to fit 7-8 components represented by the red dots in Fig. 1. The solid ellipses of Fig. 1 represent the best fit ones corresponding to parameters shown in Table 1, and the dashed ellipses correspond to 20% increase in parameters,  $I$ ,  $\lambda$ , and  $\xi$  (while holding others constant) for 3C52, 3C223.1 and 4C12.03 respectively. Hence, the role of these parameters in the formation of an ellipse is exhibited, i.e., for 4C12.03, the 20% increase in  $\xi$  from its best value changes not only the shape of the dashed ellipse, but

also its position, in which case, the morphology cannot be fitted, no matter what other parameters are.

Although making an ellipse through 7-8 points in the morphology strongly constrains the fitting parameters, we did find that the morphology of 3C223.1 can be fitted by other combination of parameters, i.e.,  $R$  approximately twice and  $I$  half of the corresponding parameters of Table 1. However, such a solution predicts much larger discrepancy in propagation time between the Northwest(NW) and Southeast(SE) structure than that of Table 1, which is contradict to the nearly symmetric structure of 3C223.1, as analyzed in Section 3. It is thus excluded.

Differentiating Eq. (2) one has,  $\Delta R_\kappa^i = \sum f_j \Delta \sigma_j$ , where  $\sigma_j$  ( $j$  from 1 to 4), denotes  $\lambda$ ,  $I$ ,  $\xi$  and  $R$  respectively, and  $f_j$  correspond to their partial differentiations respectively. If  $\Delta R_\kappa^i$ , where  $\kappa$  represents  $\alpha$  and  $\delta$  of Eq. (2), could be as large as the size of a lobe as shown by red circles in Fig. 1 (which is attributed to the error of the precession phase of a lobe), then the errors of  $\sigma_j$  can be obtained by solving four equations,  $(\Delta R_\kappa^i)^2 = \sum f_j^2 (\Delta \sigma_j)^2$ , corresponding to two lobes,  $i = 1, 2$  (the north and south), of a source. This gives conservative errors (up to 43%) to the best fit parameters of Table 1, which considerably exceed the 20% parameter errors corresponding to the deviation between the solid and dashed ellipses shown in Fig. 1.

Although the 2-dimension morphology fitting perpendicular to the LOS can give  $\eta^i$  and  $x^i$ , the most interesting parameter,  $\Omega$ , can not be extracted from Eq. (5). Since the NW and SE structure indicates that photons from them must arrive at the Earth simultaneously, this can be treated as another constraint (1-dimension), along the LOS. The two active lobes (the north and south lobes) with the shortest cooling time always satisfy  $t^1 - x^1/c = t^2 - x^2/c$ , no matter if  $t^1 \approx t^2$  ( $x^1 \approx x^2$ ), or if these values differ largely. Hence the kinematics of the two active lobes of an X-source reads,  $\eta^1 - \Omega x^1/c = \eta^2 - \Omega x^2/c$ , which includes 3-dimension

constraints, and from which  $\Omega$  can be extracted.

To obtain  $\Omega$  and its error from Eq. (5), both  $\Omega$  and  $\eta_a$  can be ordered as variables. Thus, Eq. (5) corresponds to two lines ( $i = 1, 2$ ), the cross point of which,  $(\Omega, \eta_a)$ , represents that the two signals arrive on the Earth simultaneously, as shown in Fig 3. With  $\eta^i$  and  $x^i$  of the north and south lobes obtained through morphology fitting (2-dimension), and utilize the constraint on photon arrival time (1-dimension), the cross point  $(\Omega, \eta_a)$  can be determined by Eq. (5), through which the precession velocity,  $\Omega$ , can be constrained into a small range elegantly, as shown in Table 1. The error of  $\Omega$  is determined by the errors of  $\eta^i$  and  $x^i$ , where  $\Delta x^i$  can be given by the error propagation of parameters in Table 1 via Eq. (1), and  $\Delta \eta^i$  is assumed to correspond to the “radius” of a lobe.

### 3. Asymmetry

The fitting parameters of Table 1 indicates that the phase discrepancy of the two lobes are  $\delta\eta^{12} = 185^\circ$  and  $\delta\eta^{12} = 189^\circ$  for 3C52 and 3C223.1 respectively. The  $\approx 180^\circ$  phase discrepancy corresponds to the observation of an X source through the LOS<sub>2</sub> of Fig 2. Correspondingly,  $t^1 - x^1/c = t^2 - x^2/c$  is satisfied in the case  $x^1 \approx x^2$  and  $t^1 \approx t^2$ . As the time  $t^1$  and  $t^2$  increase, the values of  $x^1$  and  $x^2$  change similarly. Therefore, the emission from the lobes and wings can arrive the Earth at approximately the same time. Consequently, the SE and NW structures of these two sources appear comparable in length and size.

In contrast to these two X-sources, the north and south lobes of 4C12.03 correspond to a phase discrepancy of  $\delta\eta^{12} = \eta^1 - \eta^2 \approx -270^\circ$  instead of  $\approx 180^\circ$ , by the fitting parameters of Table 1. This means that the photons from the active south lobe, which should differ by approximately  $\approx 180^\circ$  to the precession phase of the north lobe, have not reached the

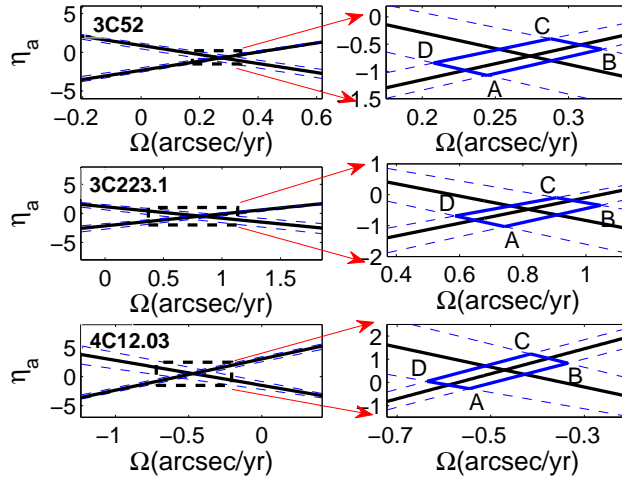


Fig. 3.— The determination of the precession period of three X-sources. The two lines that cross at  $(\Omega, \eta_a)$ , represent the same time of arrival of photons from the north and south lobes. The dashed lines correspond to uncertainty in  $\eta^i$  and  $x^i$ , estimated by the size of the lobes. The jet precession velocity of a source,  $\Omega$ , is thus constrained in the small regions, ABCD.

observer on the Earth yet ( $t^2 - x^2/c > t_a$ ), although such a lobe is observable at the core of this X-source. This corresponds to the observation of such a source through the  $\text{LOS}_1$  of Fig 2. Therefore,  $t^1 - x^1/c = t^2 - x^2/c$  is satisfied in the case  $x^1$  and  $x^2$  ( $t^1$  and  $t^2$  also) differ significantly. Such a discrepancy in  $x^1$  and  $x^2$  results in a Southwest(SW) pattern compared to that of Northeast(NE). Hence, the significant asymmetry of 4C12.03 is well understood.

The north and south lobes of 4C12.03 obviously differ in size. By the fitting parameters of Table 1, the active north lobe possesses the maximum  $t^1$  and minimum  $\eta^1$  (due to  $\Omega < 0$  in 4C12.03), which means that knots of  $t > t^1$  and  $\eta < \eta^1$  don't exist in the NE pattern at all. This is in agreement with both observers on the Earth and at the core of this X-source. Consequently, the emission of this lobe region can only be extended by the past (cooled) components, with  $t \leq t^1$  and  $\eta \geq \eta^1$ .

Contrarily, for the SW pattern, its emission can be extended by both the past components with  $t^2 - x^2/c \leq t_a$ , and by some “future” components with  $t^2 - x^2/c > t_a$ . Because components with  $t > t^2$  and  $\eta < \eta^2$  do exist near the “south lobe” (which would be observable at the core of this X-source), and the cooling emission of such “future” knots can contribute to the brightness of the “south lobe” as well by  $t_c^2 + t^2 - x_f^2/c = t_a$  (where  $x_f$  denotes the “future” emission site). Therefore, the one way extension of the NE lobe and the two way extension of the “SW lobe” lead to a larger “south lobe” than that of the NE one.

To analyze the fine asymmetry in these X-sources, Fig 4 is introduced, which is obtained as follows. Putting the obtained  $\eta^i$  and  $x^i$  through the fitting of morphologies of three sources of Fig 1 into Eq. (5), then ordering  $\Omega = \text{const}$ , the phase corresponding to the time of arrival,  $\eta_a$ , versus the phase of precession,  $\eta$ , can be obtained as shown in Fig 4, which is actually the evolution of  $t_a$  and  $t$  of the two active lobes.

As shown in Fig 4, each source has its own  $\eta - \eta_a$  curve and horizontal dashed line,  $\eta_a$ ,

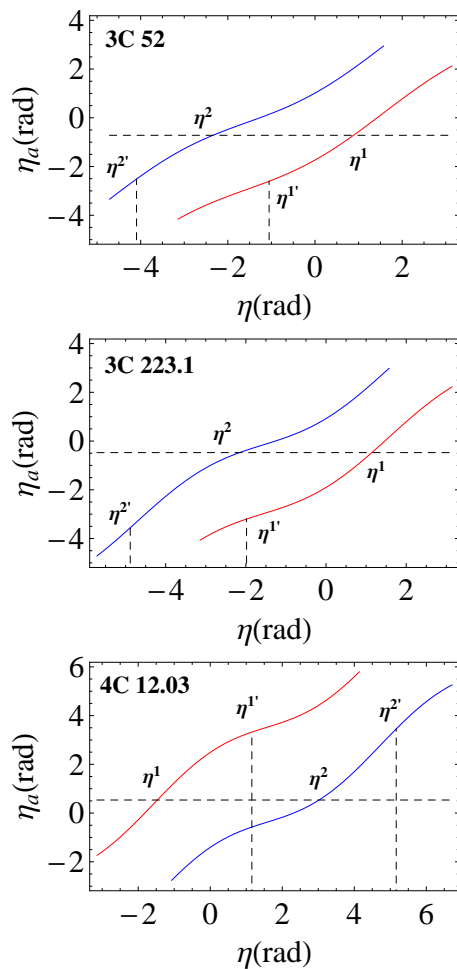


Fig. 4.— The precession phase versus the phase of arrival time, with  $\Omega = const$ . The cross points of the horizontal line with two curves,  $\eta^1$  and  $\eta^2$  corresponds to the precession phases of the north and south lobe respectively. The cross points of the curves with the vertical lines ( $\eta^{i'}$ ) correspond to the precession phase of the tail of wings.

which cross with a misalignment angle. In both 3C52 and 3C223.1, the misalignment angles of the south lobe are smaller than those of the north lobe. Moreover, the discrepancy in the misalignment angles of the north and south lobe is more obvious in 3C223.1 than in 3C 52. This explains the deviation in surface brightness of the NW and SE lobe regions in 3C223.1, as shown in Fig 1. Because the region near the south lobe is closer to the horizontal line,  $\eta_a$ , than that of the north one, which corresponds to a shorter cooling time. Hence the linking of the south lobe and its neighboring wing region has higher surface brightness than those of the north one.

#### 4. Discussion

By the fitting of Fig (1) and parameters of Table 1, precessing across the lobe-wing region takes 1.5 Myr, 0.8 Myr and 1.4 Myr for 3C52, 3C223.1 and 4C12.03 (NE pattern) respectively, the time scale of which corresponds to the cooling time discrepancy between the active lobe and the tail of wing of these sources. Interestingly, the time scale is consistent with the firm upper limits on the particle ages of 34 Myr for 3C223.1, and the estimation of the time scale of reorientation of jet axis of no more than a few Myr based on spectral gradient (Dennett-Thorpe et al. 2002).

Beside the temporary processes such as merger of SMBBH or disk instability (Merritt & Ekers 2002; Dennett-Thorpe et al. 2002), the change of jet orientation displayed in X-shaped morphology can also be originated from binary effect (Begelman et al. 1980), which can be either relativistic geodetic precession or Newtonian-driven jet precession (Katz 1997). A SMBBH system with orbital period of 20 years, and with a typical X-source black hole mass of  $5 \times 10^8 M_\odot$  (Mezcua et al. 2011) and companion mass of  $1 \times 10^7 M_\odot$ , predicts a precession period of 0.6Myr by the geodetic effect; and a precession period of 1.0Myr (with disk radius of 10 schwarzschild radius) by the Newtonian

driven effect. Consequently, the  $\sim$ Myr time scale displayed in the three X-sources can be well interpreted by either of the two binary effects. This provides another evidence to the link between X-sources and SMBBHs. Moreover, the correlation of black hole mass with X-ray luminosity and radio luminosity (Merloni et al. 2003; Falcke et al. 2004); as well as characteristic time-scale of the X-ray variability finding in AGNs and X-ray binaries (McHardy et al. 2006; K rding et al. 2007; Mirabel 2006) suggests that black hole physics likely scales with mass. The  $\sim$ Myr precession periods of the three X-sources revealed here further support such a correlation with black hole mass.

In the non-ballistic precession model, the diversity of morphology of X-sources can be simply understood by the received photons from emission sites at different precession cones. The technique is applicable to other X-sources, especially the X-shaped candidates (Cheung 2007) in the future.

## 5. Acknowledgments

We thank Y.C. Zou and Z.Q. Shen for helpful discussions. This research is supported by the National Natural Science Foundation of China, under grant NSFC10778712.



## REFERENCES

- Agudo, I. , Bach, U., Krichbaum, T. P., Marscher, A. P., Gonidakis, I. , Diamond, P. J.,  
Perucho, M., Alef, W., Graham, D. A., Witzel, A. and 4 coauthors, 2007, A&A, 476,  
L17
- Begelman, M. C., Blandford, R. D. & Rees, M. J. 1980, Nature, 287, 307
- Capetti,A., Zamfir, S., Rossi, P. , Bodo, G., Zanni, C. , & Massaglia, S. 2002, A&A, 394, 39
- Cheung, C.C. 2007, AJ, 133, 2097
- Dennett-Thorpe, J. et al. 2002, MNRAS, 330, 609
- Ekers, R. D., Fanti, R., Lari, C. & Parma, P. 1978, Nature. 276, 588
- Evans, A. S., Sanders, D. B., Surace, J. A. & Mazzarella, J. M. 1999, ApJ, 511, 730
- Falcke, H. et al. 2004, A&A, 414, 895
- Gong, B.P. 2008, MNRAS, 389,315
- E. J. Hodges-Kluck & C. S. Reynolds, arXiv:1103.4863
- Hogbom, J. A. & Carlsson, I. 1974, A&A, 34, 341
- Katz, J. I. 1997, ApJ, 478, 527
- Komossa, S. 2003, THE ASTROPHYSICS OF GRAVITATIONAL WAVE SOURCES, AIP  
Conference Proceedings, 686, 161
- Körding, E.G. et a. 2007, MNRAS, 380, 301
- Landt, H., Cheung, C. C., & Healey, S. E., 2010, MNRAS, 408, 1103
- Leahy, J. P. & Williams,A. G. 1984, MNRAS, 210, 929

- Lal D. V.&Rao, A. P. 2007, MNRAS, 374, 1085
- Lister, M. L. , Cohen, M. H., Homan, D. C., Kadler,M., Kellermann, K. I., Kovalev,Y. Y.,  
Ros, E., Savolainen,T. &Zensus, J. A. 2009, AJ, 138, 1874
- Mack, K.-H., Gregorini, L., Parma,P.,&Klein, U. 1994, A&AS, 103, 157
- Kellermann, K. I. et al. 2004, ApJ, 609, 539
- McHardy, I.M., et al. 2006, Nature, 444, 730
- Merloni, A. et al. 2003, MNRAS, 345, 1057
- Merritt,D. & Ekers, R.D. 2002, Science, 297,1310
- Mezcua, M. et al. 2011, A&A, 527, 38
- Mirabel,I. F. 2006, Proceedings IAU Symposium, 238.
- Parma, P., Ekers, R. D.,&Fanti, R. 1985, A&AS 59, 511
- Saripalli,L. & Subrahmanyam, R. 2009, ApJ, 695, 156
- Sillanpaa, A. , Haarala, S., Valtonen, M. J., Sundelius, B.&Byrd,G. G. 1988, ApJ, 325, 628
- Zhang, X.G., Dultzin-Hacyan, D.,& Wang,T. G. 2007, MNRAS, 376, 1335

Table 1: **The parameters extracted by morphology fitting and 3-dimension kinematics.**

Source	$\xi(0, 2\pi)$	$\eta^1(0, 2\pi)$	$\eta^2(0, 2\pi)$	$I(0, \pi/2)$	$\lambda^1(0, \pi/2)$	$R(0, 2)$	$\Omega(\text{arcsec/yr})$	$\Omega^{obs}(\text{arcsec/yr})$
3C52	$5.2 \pm 0.14$	$0.88 \pm 0.44$	$-2.4 \pm 0.34$	$0.52 \pm 0.065$	$0.43 \pm 0.040$	$0.40 \pm 0.093$	$0.27 \pm 0.062$	$0.21 \pm 0.048$
3C223.1	$5.1 \pm 0.061$	$1.1 \pm 0.50$	$-2.2 \pm 0.41$	$0.62 \pm 0.23$	$0.45 \pm 0.077$	$0.15 \pm 0.021$	$0.83 \pm 0.23$	$0.75 \pm 0.21$
4C12.03	$3.9 \pm 0.046$	$-1.5 \pm 0.66$	$3.1 \pm 0.50$	$0.65 \pm 0.15$	$0.35 \pm 0.079$	$0.35 \pm 0.11$	$-0.47 \pm 0.17$	$-0.41 \pm 0.15$

The precession velocities,  $\Omega$ , in the frame of the source, are inferred from Fig 3, which is related to the frame of the Earth by  $\Omega = \Omega^{obs}(1 + z)$ . The rest are precession parameters obtained by the fitting of Fig 1. Angular parameters are in rad, in which  $\eta^1$  and  $\eta^2$  represent the phase of the north and south lobe respectively. The opening angle of precession cone,  $\lambda^1$ , corresponds to the NW(NE for 4C12.03) pattern, and the opposite pattern is fitted by  $\lambda^2 = \pi - \lambda^1$ . The distance  $R$  is in Mpc, which is obtained by multiplying the arcsec value (through morphology fitting) by the angular size distance (through the cosmology parameters and the measured redshift).